Desalination and Water Treatment
www.deswater.com

7 (2009) 25–34

1944-3994 / 1944-3986

An experimental and modeling study of nanofiltration processes for mixed electrolyte solutions

S.A. Avlonitis*, D.A. Avlonitis, S. Skourtis, D. Vlachos

Laboratory of Quality Control, Operations Management and Process Engineering, Department of Mechanical Engineering, Technological Educational Institution (T.E.I.) of Chalkida, 34400 Psaxna, Evia, Greece
Tel. +30 (22280) 99650; Fax +30 (22280) 99649; email savlon@teihal.gr

Received 15 July 2008; accepted in revised form 15 June 2009

ABSTRACT

An experimental and modeling procedure is presented for the investigation of the performance of nanofiltration membranes. The proposed procedure may be applied to nanofiltration membrane system operating with mixed salts solutions to estimate the flux and quality of the permeate water. The model had been proven successful in the past for the study of RO systems and is based on the analytical equations of the two dimensional flow. It contains a set of five constants that are case-specific and have to be determined. Two of these constants were determined by forcing agreement of the model to appropriate experimental data while the rest were calculated from established generalized correlations. A number of pilot plant experiments were conducted using TRISEP (4040-XN45-TSF) nanofiltration membrane with mixed salts solutions differing in composition and in temperature. A set of the data obtained by these experiments has been used for fixing the parameters of the model while the remaining sets were used for evaluation of the performance of the model. The method is consistent and robust and as it is demonstrated, the predictions of the model are in excellent agreement to the experimental data. It is believed, therefore, that the proposed procedure is useful in cases where predictions of nanofiltration membrane performance are required.

Keywords: Nanofiltration; Modelling; Experimental data; NF performance

1. Introduction

The shortage of clean water worldwide has made industrial wastewater treatment before disposal an important necessity. Strict rules and regulations for the disposal of industrial wastewater have been implemented worldwide due to a steadily increasing public concern. In particular, the removal of pollutants from the water disposed to the environment has become an environmental issue. Industrial wastes are resistant to physical degradation while at the same time the reuse of industrial wastewater, particularly for high water consuming industries, could relieve underground water reservoirs. On the other hand, the shortage and the high cost of water forces the industry to pay serious attention to the appropriate treatment of the produced effluents and the reuse of the water. For example, the wastewater generated by the textile industry is one of the most polluting among in the industrial sector, with high organic and mixed salts contents.

Nanofiltration (NF) is a pressure-driven membrane separation process that has been applied to address this worldwide issue. The relatively low operating pressure and the improved separation properties have made NF

* Corresponding author.

very attractive among other membrane separation processes, such as ultrafiltration (UF) and reverse osmosis (RO). NF process combines higher rejection properties than UF at higher pressure and lower flux and lower applied pressure than RO at lower rejection properties. Most commercial NF membranes are thin-film synthetic polymers composites containing charged groups [1,2] with pore size approximately one nanometer. It appears that the separation performance of NF membranes is controlled by steric effects, Donnan equilibria, dielectric and transport phenomena. NF is a mostly suitable process for the separation of several inorganic (hardness, nitrates, phosphates, heavy metals, etc.) and organic (bacteria, viruses, pesticides, hormones, flavours, antibiotics, etc.) substances from natural or industrial waters.

The optimization and characterization of the NF process requires the mathematical formulation and the development of good predictive models. The mathematical models for reverse osmosis (RO) and nanofiltration available in the literature are based either on transport mechanisms or irreversible thermodynamics. The models may be classified in four categories:

1. Those based on solution-diffusion model [3]
2. Extended Nerst–Plank models [4–6]
3. The Hagen–Poiseuille models [7,8]
4. Other than solution–diffusion model based on irreversible thermodynamics, [9–13].

The solution–diffusion model for RO and NF is based on transport mechanism, i.e. the solutes and water are dissolved in the membrane material and they diffuse at different rates through the membrane due to the concentration gradients. The solution–diffusion model has been extensively used in predicting the performance of separation systems with high solute rejection properties.

The extended Nerst–Plank model is the most elaborate model for transport of multiple ions through the charged nanofiltration membrane. This model describes the three important mechanisms of ionic transport in the membranes: (a) diffusion and (b) electromigration as a result of concentration and electrical potential gradients, respectively, and (c) convection caused by the pressure difference across the membrane [14].

The Hagen–Poiseuille model is commonly used for microfiltration and ultrafiltration processes, where aqueous systems are permeating through porous media. The model has been modified for applications in RO and NF membranes [8,15].

The models derived from the irreversible thermodynamics are the Kedem–Katchalsky model and Spiegler–Kedem model [16]. In these models the membrane is treated as a black box in which relatively slow processes proceed near the equilibrium without specific transport mechanisms and structure of the membrane. The model simply considers that the fluxes of solute and solvent are directly related to the chemical potential differences between the two sides of the membrane.

All of the above models can make very good predictions in the case of simple aqueous systems such as small molecule separations and simple salt separations. However, in most industrial cases the treated solution by NF membranes is a multi-component aqueous solution and the rejection characteristics of the membrane for each individual component are affected by the presence of the others. In the last few years, more attention has been paid to the separation performance of the NF membranes for the mixed salts solution [14], and for three kinds of ions [17], but there is still lack of knowledge for the separation performance of NF membranes with the mixed salt solutions. The challenge addressed by the present work is to develop a mathematical model to include more complex multi-component separations and to validate the model's predictions using separations of real industrial interest.

The separation performance of an NF membrane, such as the rejection and the permeation flux, is usually described by the membrane parameters, i.e. the reflection coefficient and the solute permeability, according to the Spiegler–Kedem model. Based on the solution–diffusion model a five-parameter approach can be used (water permeation coefficient, salt permeation coefficient, mass transfer coefficient, brine friction parameter and permeate friction parameter) to formulate the RO performance [18–20].

The above five-parameter model is applied in this work for the evaluation of the separation characteristics and the performance of NF membranes operating with mixed salt solutions. The mathematical model was based on our previous work on the RO process. Two of the five parameters of the model were determined by forcing agreement of the model to appropriate experimental data with distilled water and with mixed salts solutions. Then the validation of the model was carried out by comparing predictions with experimental data of one commercial NF membrane (TRISEP 4040-XN45-TSF) operating with mixed salts solutions. The developed model in the form of a computer program may be used to evaluate the separation performance of commercial NF membranes in operating conditions as long as the geometrical characteristics of the membrane and the five parameters of the proposed model have previously been obtained.

2. The mathematical model

The physical phenomena are approximated with the following assumption and approximations as in Table 1.

The mathematical model is comprised from the following equations:

The average volumetric water flux, J, is calculated from the following equation:

Table 1
Assumptions and approximations for the 2-dimensional flow model

1	Validity of Darcy's law for the permeate and the brine channel.
2	Validity of solution–diffusion model for the transport of water through the membrane. No flow restrictions for the locally produced permeate in the porous substructure of the composite membrane.
3	Immediate and complete mixing of the locally produced permeate water with the bulk flow in the permeate channel.
4	The permeate concentration has been neglected in comparison to the feed concentration.
5	Membrane modules are made up of flat channels, with constant geometrical shape, as detailed in Appendix I.
6	Constant fluid properties.
7	Negligible velocities of brine and permeate components along the y (tangential) and x (axial) axis respectively.
8	Negligible diffusive mass transport along the x and y direction in both channels. This means that the flux through the membrane due to diffusion is much smaller to the flux due to convection. The driving force for the water transport is the effective pressure across the membrane.
9	The brine concentration varies linearly with the distance x ($0 \le x \le L$) in the axial direction. $$c_b(x) = c_f + fx \quad \text{(A1)}$$ where $$f = \frac{c_b(L) - c_f}{L} \quad \text{(A2)}$$ The value of f is an indication of the recovery ratio R.
10	Validity of the thin film theory, with the approximation given by the following equation: $$c_{bw}(x) = \left[1 + \frac{J}{k} + \frac{1}{2}\left(\frac{J}{k}\right)^2\right] c_b(x) \quad \text{(A3)}$$
11	Constant mass transfer coefficient, k, given by Eq. (A4) $$\mathrm{Sh} = 0.63 \times \mathrm{Sc}^{0.17} \times \mathrm{Re}_f^{0.40} \times \left[\frac{c_f}{\rho}\right]^{-0.77} \times \left[\frac{P_f}{P_o}\right]^{-0.55} \quad \text{(A4)}$$ where ρ is the density of the solution and P_o is the atmospheric pressure.
12	Osmotic pressure proportional to the concentration, according to the following equation: $$\pi = \omega \cdot c \quad \text{(A5)}$$

$$J = \frac{q \tanh\frac{w}{q}}{\omega f w L}\left\{\left(k + k_1\omega c_f\right)\ln\frac{k + k_1\omega c_b(L)}{k + k_1\omega c_f}\left[\Delta P_{ef}(0,w) + \frac{k}{k_1}\right] - k\omega\left[c_b(L) - c_f\right]\right.$$
$$\left. + \frac{c_f u_f k_{fb}\mu}{f}\left[k_1\omega\left(c_b(L)\right) - c_f\right] - k\ln\frac{c_b(L)}{c_f}\ln\frac{k + k_1\omega c_B(L)}{k} - \frac{k_1^2\omega^2}{4k}\left(c_b^2(L) - c_f^2\right)\right\} \quad (1)$$

The average salt flux, J_2, is provided by the following equation:

$$J_2 = \frac{k_2}{wL}\left\{c_f wL + \frac{fL^2 w}{2} + \frac{q\tanh\frac{w}{q}}{k_1 f\omega^2 k} \times \left\{k_1\omega\left(c_b(L) - c_f\right)\left[\Delta P_{ef}(0,w)\left(k + k_1\omega c_f\right) + \frac{k^2}{k_1} - \frac{k\omega\left(c_b(L) - c_f\right)}{2}\right]\right.\right.$$
$$-k(k + k_1\omega c_f) \times \ln\frac{k + k_1\omega c_b(L)}{k + k_1\omega c_f}\left[\Delta P_{ef}(0,w) + \frac{k}{k_1}\right] + \frac{k c_f u_f k_{fb}\mu \ln\frac{c_b(L)}{c_f}}{f}\left[k\ln\frac{k + k_1\omega c_b(L)}{k} - k_1\omega c_b(L)\right.$$
$$\left.\left.\left. + \frac{k_1^2\omega^2}{4k}\left(c_b^2(L) - c_f^2\right)\right]\right]\right\} \quad (2)$$

where

$$\Delta P_{ef}(0,w) = \frac{\left(\Delta P - \omega c_f\right) k}{k + k_1 \omega c_f} \quad (3)$$

and

$$q = \sqrt{\frac{h_p}{2k_1 k_{fp} \mu}} \quad (4)$$

Eqs. (1) and (2) have been presented in previous works for the RO process [19,20]. In these two equations, (1) and (2), the pressure in the permeate and brine channel, P_p and P_b, the concentration polarization, c_{bw}, and the local concentration, c_f, along each membrane module have been taken into account along with the assumptions and approximations given in Table 1.

For the meaning of the symbols appearing in the above equations see the list of symbols.

The average salt flux, J_1 is related to the volumetric average water flux, J, according to Eq. (5).

$$J_2 = J c_p \quad (5)$$

The permeate flow rate, Q_p, can be found as the product of the total active membrane area (excluding the glued areas of the membrane) and the volumetric average water flux.

Taking into account that all the membrane makers are using similar feed and permeate spacers, the brine friction parameter, k_{fb}, was assumed to be given by Eq. (6) and the permeate friction parameter, k_{fp} by Eq. (7), as suggested by Avlonitis et al. [18]:

$$k_{fb} = 309 \times \mathrm{Re}_f^{0.83} \quad (6)$$

$$k_{fp} = 462,915 \times \mathrm{Re}_p^{0.26} \quad (7)$$

The membrane permeability coefficient for each different type of membrane, k_1, can be expressed as a function of pressure and temperature by Eq. (8) and the salt permeability coefficient by Eq. (9), as suggested by Avlonitis et al. [18]:

$$k_1^T = k_{1,0}^T e^{a_P P(0,w)} \quad (8a)$$

where $k_{1,0}^T$ is the extrapolated value of k_1^T when $P(0,w)$ is zero and α_p is a constant in bar^{-1}.

$$k_{1,0}^T = k_{1,0}^{20}\, e^{a_T\left(\frac{T-T_{20}}{T_{20}}\right)} \quad (8b)$$

$$k_2 = k_2^0\, e^{b_T \frac{T-T_o}{T_o}} \quad (9)$$

where $k_{1,0}^{20}$ and k_2^0 are constants depending on the membrane type.

The k_1 values can be determined by running experiments with distilled water at different temperatures and applied pressures and then solve the following Eq. (10) numerically [18].

$$J = \frac{k_1 q \tanh\frac{w}{q}\left\{b\Delta P_{eff}^2(0,w)\sinh(aL) + \frac{u_f^2}{b}\left[1-\cosh(aL)\right] + \Delta P_{ef}(0,w)\left[1-e^{-aL}\right]\right\}}{awL\,\left[b\Delta P_{ef}(0,w) + u_f\right]} \quad (10)$$

where

$$a = \sqrt{\frac{2k_1 k_{fb}\mu}{h_b}} \quad (11)$$

and

$$b = \sqrt{\frac{2k_1}{k_{fb}\mu\, h_b}} \quad (12)$$

Values of $k_2(T)$ can be evaluated by running experiments at several temperatures with salt water solutions and then using Eq. (2).

When all five parameters were determined then Eqs. (1), (2) and (5) were deployed to determine the permeate flow rate and the permeate quality for each individual membrane module.

3. Methods and materials

Three different sets of experimental data were collected during the operation of the pilot plant and were subsequently analyzed by our model, as follows:

a. Experiments with distilled water at different temperatures and pressures to determine the water permeability coefficient of the membrane TRISEP 4040-XN45-TSF, k_1, by using Eqs. (6), (7), (10), (11) and (12).
b. Experiments with mixed solute solutions to determine the salt permeability coefficient of the membrane TRISEP 4040-XN45-TSF, k_2, by using Eqs. (A1)–(A5) and Eq. (2).
c. Experiments with mixed salts solutions to evaluate the predictions of the membrane performance of the proposed model as detailed by Avlonitis et al. [19].

The recovery, R, of the membrane is defined as follows:

$$R = \frac{Q_p}{Q_f} \times 100 \quad (13)$$

where Q_p is the permeate flow rate and Q_f is the feed flow rate.

The rejection properties of the membrane is estimated by the rejection, r,

$$r = \frac{c_f - c_p}{c_f} \times 100 = \left(1 - \frac{c_p}{c_f}\right) \times 100 \quad (14)$$

where c_p is the permeate concentration and c_f is the feed concentration.

3.1. Experimental setup

All experiments were conducted on pilot plant scale. A SCADA system was installed to the plant so that long term experiments could be performed while the data were continually recorded. The measuring devices were

1. Two pressure transducers, WIKA model OC-1, 0–25 bar, accuracy < 1% of span.
2. Two paddle wheel flow meters, GF F3.00 Paddlewheel flow sensor and F9.00 flow monitor and transmitter.
3. One conductivity meter, JUMO type 202540.
4. One thermocouple.

The flow diagram of the pilot plant is illustrated in Fig. 1. The readings were verified every time manually by the use of conductivity meter, Bourdon manometers, pH meter and timer and measuring cylinder for the flow rates. The concentration of the test solution was kept constant by recycling the permeate into the feed tank. The temperature of the solution was controlled and kept constant at any desired value by a cooler and a heater. During each experimental run, samples were taken from the sampling ports and they were analyzed manually. The circulation pump was electronically controlled to stabilize downstream pressure at any preset value. The valves could control the flow rates and the recovery, while the pressure was kept constant.

3.2. Materials

The compositions of the mixed salts solutions used in the experiments are presented in Table 2. The synthetic mixture on laboratory scale was prepared by the use of distilled water and appropriate quantities of salts and it was set in a polypropylene tank. The salt concentration (TDS) was related to the conductivity by the use of standard solutions, as shown in Table 3. The No. 1 experimental concentration is a standard effluent of the dye industries while the two others experimental concentrations are much higher.

The nanofiltration membranes were 4 inch modules made by TRISEP (4040-XN45-TSF). According to their manufacturer's specifications, these membranes have minimum rejection for $MgSO_4$ and sucrose 92% at solute concentration 2000 ppm and operating pressure 100 psi.

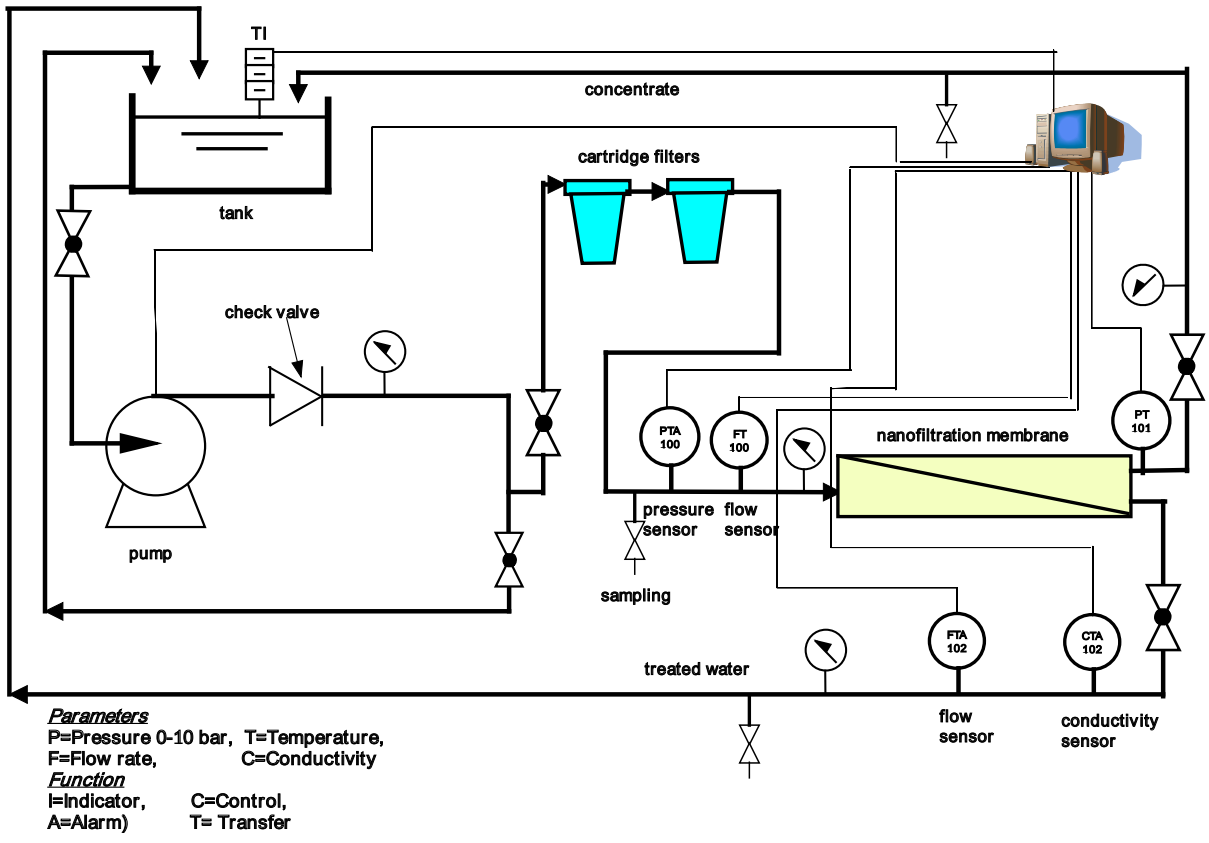

Fig. 1. Flow diagram of the nanofiltration pilot plant.

Table 2
Composition of the multiple solutes system at 20°C

Substance	Feed solution, experimental run		
	No. 1	No. 2	No. 3
$CaCl_2$, mg/l	200	500	1000
NaCl, mg/l	500	1000	2000
$(NH_4)_2SO_4$, mg/l	500	1000	2000
Total conductivity at 20°C, μS/cm	1800	3820	7050
pH	7.10	7.15	7.20
Hardness as mg CaO	110	255	485

Table 3
Correlation equations for conductivity and TDS

Temperature (°C)	Correlation equation
20	TDS = –23 + 0.64 × conductivity
25	TDS = –23 + 0.62 × conductivity
30	TDS = –16 + 0.61 × conductivity

The maximum recommended recovery is 15%. However, much higher recoveries were used to test the performance of the membrane at extreme conditions. In a pretreatment stage two cartridge filters, one of 20 μm and one of 5 μm, were used.

3.3. Instrumentation and analyses

For every run a feed solution was prepared having the desired concentration and pH. The pilot plant was then run until the desired temperature was reached and then readings were taken and recorded both manually and automatically by the SCADA system. The pH of the solutions was measured by a pH meter supplied by Hoezle & Chelius KG. The conductivity and the total salt concentrations of the solutions were determined by a conductivity meter supplied by Hanna (model HI 8733). The permeate and brine flow rates were measured by paddle wheel flow meters and timer with measuring cylinder. The temperature was measured by a thermocouple. Pressure transducers and Bourdon manometers were used to measure the pressures. The concentrations of Ca^{2+} and CO_3^{2-} were determined by titration.

3.4. Experimental data for the determination of the parameters of the model

The first set of experiments was run with distilled water. The experimental data and the calculated values for TRISEP 4040-XN45-TSF nanofiltration membrane are given in Table 4. The second set of experiments concerns No. 1 mixed salt solution, the characteristics of which are presented in Table 2.

The measured experimental values and the calculated values of k_2 for TRISEP 4040-XN45-TSF nanofiltration membrane are presented in Table 5. Readings were taken when the corresponding indications were stable at least for 15 min. The composition of the feed was tested periodically and it was adjusted accordingly.

3.5. Experimental data for the validation of the model

The third set of experiments concerns mixed salt solutions at higher concentration, that is No. 2 and No. 3 in Table 2. These data were used next for the validation of the theoretical model of this work. At the end of the experimental work, the membrane was opened and its dimensions were measured. These data are given in Appendix I.

4. Results and discussion

Eq. (8a) can be written in the following linear form:

$$\ln k_1^{\Phi} = \ln k_{1,0} - \alpha_p P(0,w) \quad (15)$$

Table 4
Experimental data and calculated values of k_{fb}, k_{fp}, k_1 with distilled water

Experimental				Calculated		
T (°C)	$P_f(0,w)$ (bar)	Q_f (l h^{-1})	Q_p (l h^{-1})	k_{fb} (cm^{-2})	k_{fp} (cm^{-2})	k_1 (cm s^{-1} bar^{-1})
20	4.0	2020	125	16,124	834,077	2.42×10^{-4}
20	6.0	1615	200	13,391	938,052	2.31×10^{-4}
20	8.0	987	270	6,587	1011,163	2.22×10^{-4}
25	4.0	2027	150	17,839	872,978	3.02×10^{-4}
25	6.0	1600	240	14,658	981,823	2.89×10^{-4}
25	8.0	862	335	8,773	1067,030	2.93×10^{-4}
30	4.0	2033	185	19,580	919,967	3.96×10^{-4}
30	6.0	1570	305	15,743	1042,443	4.00×10^{-4}
30	8.0	855	415	9,541	1125,202	3.90×10^{-4}

Table 5
Experimental data and calculated values of k and k_2 with mixed salt solutions

Experimental						Calculated	
T (°C)	$P_f(0,w)$ (bar)	Q_f (l h^{-1})	Q_p (l h^{-1})	Q_f (lt h^{-1})	c_p[†] (mg l^{-1})	k (cm s^{-1})	k_2 (cm s^{-1})
20	4.0	1200[*]	66,1	2080	100	0.219	2.70×10^{-5}
20	6.0	1200[*]	116,1	1610	80	0.159	3.43×10^{-5}
20	8.0	1200[*]	163,0	930	56	0.108	3.03×10^{-5}
25	4.0	1200[*]	84,0	2030	162	0.248	3.50×10^{-5}
25	6.0	1200[*]	144,0	1600	104	0.180	5.58×10^{-5}
25	8.0	1200[*]	200,0	910	84	0.123	5.53×10^{-5}
30	4.0	1200[*]	102,0	2035	232	0.281	11.66×10^{-5}
30	6.0	1200[*]	180,0	1560	161	0.202	11.88×10^{-5}
30	8.0	1200[*]	250,0	870	130	0.137	10.58×10^{-5}

[*] Calculated from the data No. 1 of Table 2.
[†] In every case the rejection of the hardness was more than 97%.

Table 6
Experimental data for mixed salt solutions

T (°C)	$P_f(0,w)$ (bar)	c_f (mg l^{-1})	Q_p (l h^{-1})	Q_f (l h^{-1})	c_p[†] (mg l^{-1})
20	4.0	2500[*]	53	2036	330
20	6.0	2500[*]	104	1600	250
20	8.0	2500[*]	156	902	150
20	6.0	5000[*]	75	1610	630
20	8.0	5000[*]	120	938	500

[*] Calculated from data No. 2 of Table 2.
[§] Calculated from data No. 3 of Table 2.
[†] In every case the rejection of the hardness was more than 99%.

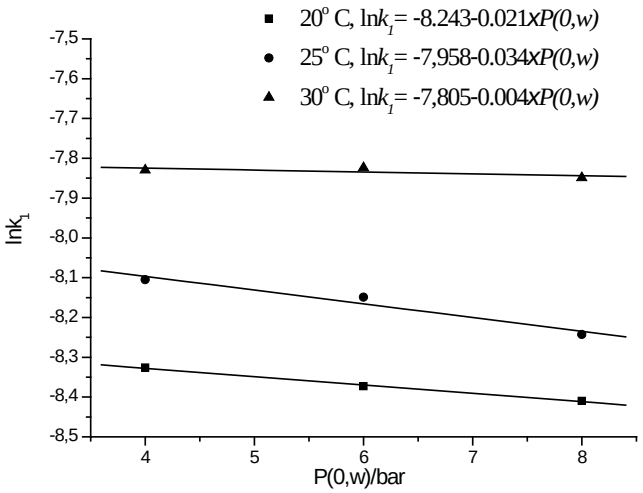

Fig. 2. Experimental and calculated values of lnk_1 vs. pressure at different temperatures.

The graphs of Eq. (15) at different temperatures and the correlation equations are illustrated in Fig. 2 together with data collected from Table 4.

In all cases the statistical analysis gives a standard error for intercept values between 0.008–0.044 and for the slope values between 0.001–0.007. From Fig. 2 it appears that on average $k^T_{1,0} = 2.63\times10^{-4}$cm s^{-1} bar^{-1} and $\alpha_p = 0.018$ bar^{-1}.

A similar procedure is applied for Eq. (8b) from which one can have:

$$\ln k^T_{1,0} = \ln k^{20}_{1,0} + \alpha_T \frac{T - T_{20}}{T_{20}} \quad (16)$$

In Fig. 3 experimental data and lines obtained from Eq. (16) and fitted to them are presented.

From Fig. 3 it appears that on average $k^{20}{}_{1,0} = 2.20\times10^{-4}$ and $\alpha_T = 1.2$. A combination of Eqs. (8a) and (8b) yields the following equation which gives the water permeability coefficient, k_1, at any pressure and temperature:

$$k_1 = 2.20\times10^{-4}\, e^{1.2\times\left(\frac{T-T_{20}}{T_{20}}\right)-0,016\times P(0,w)} \quad (17)$$

Eq. (9) can be transformed to the following form:

$$\ln k_2^T = \ln k_2^0 + \beta_T \frac{T - T_0}{T_0} \quad (18)$$

If the calculated values from Table 5 are used then the following graph (Fig. 4) can give the values of $k_2{}^0$ and β_T as 2.75×10^{-5} and 2.63 respectively.

Consequently Eq. (9) is reduced to the following form:

$$k_2 = 2.75\times10^{-5}\, e^{2.63\,\frac{T-T_o}{T_o}} \quad (19)$$

In summary, the membrane efficiency and performance was tested at different operating conditions. The

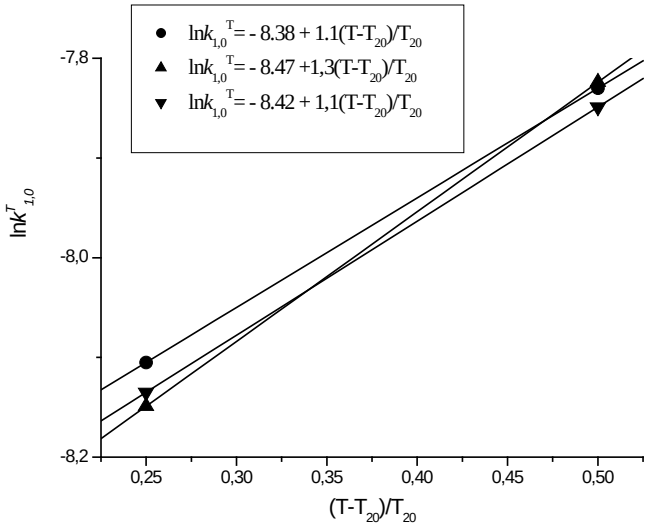

Fig. 3. Experimental and calculated values of $\ln k^T_1$ vs. the relative increase in temperature.

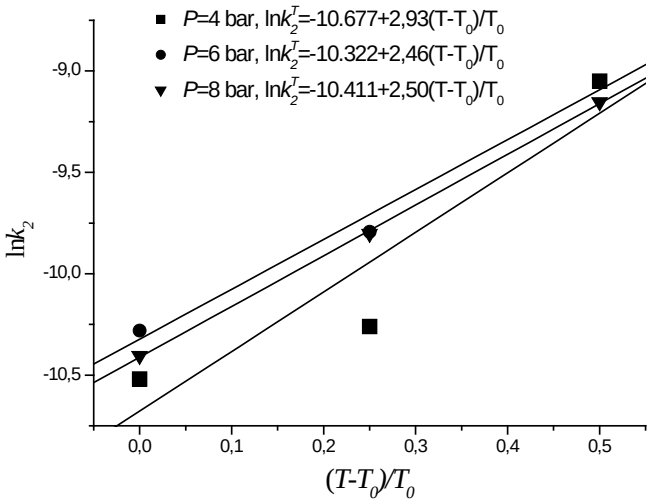

Fig. 4. Experimental and calculated values of $\ln k_2$ vs. the relative increase in temperature.

applied pressure was varied from 4 to 8 bar and the recovery from 2.6 to 28.7% while the total rejection of all ions is between 84–94% depending on the operating conditions and feed concentration. The predictions of our model, which integrates all of the above equations for the five parameters, are presented in Table 7 along with the experimental data. A very good agreement was found between experimental data and predictions. The maximum deviations between experimental data and predictions were 9%.

It can be alleged that the same simple procedure can be applied for membrane modules in series, as they are in the real industrial membrane pressure vessels, according the procedure that was applied for the RO membranes [20]. Simple mass balances can be used to give the permeate flow rate and permeate quality when more than one membrane modules are in series. The relevant equations are:

$$Q_p = Q_{p1} + Q_{p2} + \ldots + Q_{pt}, \quad c_p = \frac{\sum_{i=1}^{t} c_{pi} Q_{pi}}{Q_p} \tag{20}$$

and $Q_{fi} = Q_{f(i-1)} - Q_{p(i-1)}$

5. Conclusions

An explicit approach for the nanofiltration processes modelling of mixed salt solution has been detailed. The proposed methodology can provide reliable predictions for the nanofiltration membranes performance irrespective of the specific type. The mixed salt solution was treated as a homogenous solution characterized by its total concentration, i.e. the present approach does not account for the possible interactions of the different ions on the performance of the nanofiltration membranes. Though this issue has not been examined in the present work, nonetheless, it is evident that the estimated values of the model parameters are independent of the reference solution concentration and temperature. Therefore, the five parameters model is useful for the prediction of nanofiltration membrane process performance for mixed salts solutions when the permeate flux and the permeate quality are of interest.

Table 7
Experimental data and predictions from the proposed model for mixed salt solutions at 20°C

P_f (bar)	c_f (mg l^{-1})	Q_f (l h^{-1})	Q_p (l h^{-1})		TDS$_p$ (mg l^{-1})	
			Experimental	Prediction	Experimental	Prediction
4.0	2500	2036	45	42	455	494
6.0	2500	1600	110	116	195	187
8.0	2500	902	165	180	130	132
6.0	5000	1610	50	48	840	872
8.0	5000	938	120	111	420	409

Symbols

b — Constant defined by Eq. (12), m s^{-1} bar^{-1}
c — Concentration, kg m^{-1}
D — Diffusion coefficient, m^{2}s^{-1}
f — Constant defined by Eq. (A2), kg m^{-4}
ΔP_{ef} — Driving pressure, bar
ΔP — Pressure difference given by ($P_f(0,w)$–$P_p(0,w)$), bar
h — Height, m
J — Average volumetric flux, m s^{-1}
J_2 — Average solute mass flux, kg m^{-2} s^{-1}
k — Mass transfer coefficient, m s^{-1}
k_1 — Water permeability coefficient, m s^{-1} bar^{-1}
$k_{1,0}$ — Water permeability coefficient at zero pressure, m s^{-1} bar^{-1}
$k_{1,0}^{20}$ — Water permeability coefficient at 20°C, m s^{-1} bar^{-1}
$k_{1,0}^{T}$ — Water permeability coefficient at T K, m s^{-1} bar^{-1}
k_2 — Solute permeability coefficient, m s^{-1}
k_2^T — Solute permeability coefficient at any temperature, m s^{-1}
k_f — Friction parameter, m^{-2}
L — Membrane length (axial), m
L_2 — Membrane length with glue, m
P — Pressure, Pa
P_f — Applied pressure at the inlet of the pressure vessel, Pa
P_o — Constant (10^5 Pa)
q — Constant for a given membrane and temperature defined by Eq. (4), m
Q — Flow rate, m^3/s
Re — Reynolds number (Re = $h_b u_b \varrho/\mu$)
Sc — Schmidt number (Sc = $\mu/\varrho D$)
Sh — Sherwood number (Sh = kh_b/D)
T — Temperature, K
u — Velocity, m/s
w — Membrane width (tangential), m
w_2 — Membrane width with glue, m
x — Coordinate along the membrane length, m
y — Coordinate along the membrane width, m

Greek

α — Constant defined by Eq. (11), cm^{-1}
α_p — Constant defined by Eq. (8a), bar^{-1}
α_T — Constant defined by Eq. (8b), bar^{-1}
μ — Viscosity, kg m^{-1} s^{-1}
π — Osmotic pressure, Pa
ϱ — Density, kg/m^3
ω — Osmotic pressure coefficient, N m kg^{-1}

Subscripts

b — Brine
ef — Effective
f — Feed
m — Membrane
p — Permeate
w — Wall

References

[1] R. Rautenbach and A. Groschl, Separation potential of nanofiltration membranes, Desalination, 77 (1990) 73.
[2] P. Schirg and F. Widmer, Characterization of nanofiltration membranes for the separation of aqueous dye-salt solutions, Desalination, 89 (1992) 89.
[3] J.G. Wijmans and R.W. Baker, The solution diffusion model: A review, J. Membr. Sci., 107 (1995) 1–21.
[4] W.R. Bowen and J.S. Welfoot, Predictive modeling of nanofiltration: membrane specification and process optimization, Desalination, 147 (2002) 197–203.
[5] W.R. Bowen, B. Cassey, P. Jones and D.L. Oatley, Modeling the performance of membrane nanofiltration-application to an industrially relevant separation, J. Membr. Sci., 242 (2004) 211–220.
[6] J. Garcia-Aleman and J.M. Dickson, Mathematical modeling of nanofiltration membranes with mixed electrolyte solutions, J. Membr. Sci., 235 (2004) 1–13.
[7] M. Mulder, Basic principles of membrane technology, Kluwer, Dordrecht, 1996, pp. 224–225.
[8] J. Geens, B. Van der Bruggen and C. Vandecasteele, Transport model for solvent permeation through nanofiltration membranes, Separ. Purif. Technol., 48 (2006) 255–263.
[9] O. Kedem and A. Katchalsky, Permeability of composite membranes, Part 1. Electric current, volume flow and flow of solutes through membranes, Trans. Faraday Soc., 59 (1963) 163–174.
[10] K.S. Spiegler and O. Kedem, Thermodynamics of hyperfiltration (RO) criteria for efficient membranes, Desalination, 1 (1966) 311–326.
[11] S. Wadley, C.J. Brouckaert, L.A.D. Baddock and C.A. Buckly, Modeling of nanofiltration applied to the recovery of salt from waste brine at a sugar decolourization plant, J. Membr. Sci., 102 (1995) 163–175
[12] A. Bhattacharya and P. Ghosh, Nanofiltration and reverse osmosis membranes, theory and application in separation of electrolytes, Rev. Chem. Eng., 20 (2004) 111–173.
[13] A.L. Ahmad, M.F. Chong and S. Bhatia, Mathematical modeling and simulation of the multiple solutes system for nanofiltration process, J. Membr. Sci., 253 (2005) 103–115.
[14] J. Garcia-Aleman and J.M. Dickson, Permeation of mixed-salt solutions with commercial and pore-filled nanofiltration membranes: membrane charge inversion phenomena, J. Membr. Sci., 239 (2004) 163.
[15] G. Jonsson and C.E. Boesen, Water and solute transport through cellulose acetate reverse osmosis membranes, Desalination, 17 (1975) 145–165.
[16] S. Kimura, Analysis of reverse osmosis membrane behaviors in a long term verification test, Desalination, 100 (1995) 77–84.
[17] S. Choi, Z. Yun, S. Hong and K. Ahn, The effect of co-existing ions and surface characteristics of nanomembranes on the removal of nitrate and fluoride, Desalination, 133 (2001) 53.
[18] S. Avlonitis, W.T. Hanbury and M. Ben Budinar, Spiral wound modules performance. An analytical solution: Part I, Desalination, 81 (1991) 191–208.
[19] S. Avlonitis, W.T. Hanbury and M. Ben Budinar, Spiral wound modules performance. An analytical solution: Part II, Desalination, 89 (1993) 227–246.
[20] S. Avlonitis, M. Pappas and K. Moutesidis, A unified model for the detailed investigation of membrane modules and RO plants performance, Desalination, 203 (2007) 218–228.

Appendix 1

Dimensions of the 4'' TRISEP 4040-XN45-TSF nanofiltration membrane

Permeate channel height, mm	$h_p = 0.24$
Brine channel height, mm	$h_b = 0.68$
Membrane height, mm	$h_m = 0.16$
Total membrane length, cm	$L_2 = 92.0$
Active membrane length, cm	$L = 82.0$
Total membrane width, cm	$w_2 = 95.0$
Active membrane width, cm	$w = 85.0$
Active membrane area, m^2	$A = 6.97$
Number of leaves in 4'' 4040-XN45-TSF	N= 5

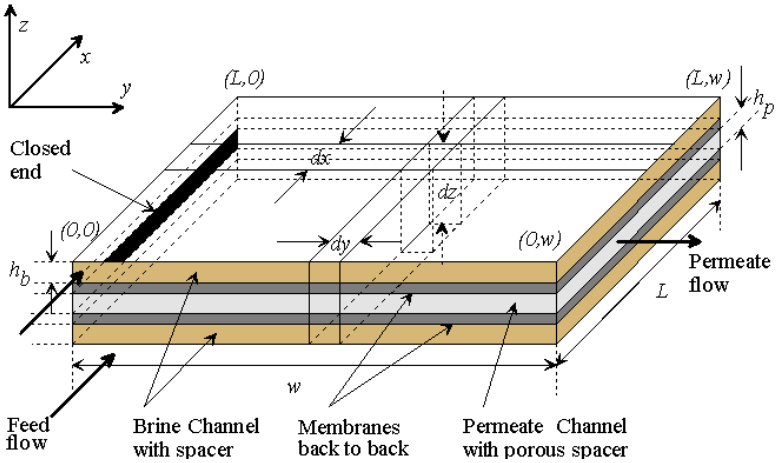

Fig. I.1 Unwound spiral wound RO membrane module.